Chemical Physics 375 (2010) 578–586

Contents lists available at ScienceDirect

Chemical Physics

journal homepage: www.elsevier.com/locate/chemphys

Transport of free surface liquid films and drops by external ratchets and self-ratcheting mechanisms

Uwe Thiele [a,*], Karin John [b]

[a] Department of Mathematical Sciences, Loughborough University, Loughborough, Leicestershire LE11 3TU, UK
[b] Laboratoire de Spectrométrie Physique UMR 5588, CNRS and Université Joseph Fourier, Grenoble I, BP 87, 38402 Saint-Martin-d'Hères, France

ARTICLE INFO

Article history:
Received 21 January 2010
In final form 11 July 2010
Available online 14 July 2010

Keywords:
Fluid ratchets
Droplet transport
Heterogeneous substrates
Vibrated substrates
Microfluidics

ABSTRACT

We discuss the usage of ratchet mechanisms to transport a continuous phase in several micro-fluidic settings. In particular, we study the transport of a dielectric liquid in a heterogeneous ratchet capacitor that is periodically switched on and off. The second system consists of drops on a solid substrate that are transported by different types of harmonic substrate vibrations. We argue that the latter can be seen as a self-ratcheting process and discuss analogies between the employed class of thin film equations and Fokker–Planck equations for transport of discrete objects in a 'particle ratchet'.

1. Introduction

Most of the many studied ratchet mechanisms are discussed in the context of directed transport and filtering of discrete objects as, e.g., colloids or macromolecules [1]. Examples include colloidal particles, that move in a directed manner through an array of periodic asymmetric micropores when under the influence of an oscillating external pressure [2]. Such particles may as well be driven by a dielectric potential of sawtooth shape that is switched on and off periodically [3]. In many of these 'discrete' ratchets the carrier fluid (or solvent) does not or nearly not move on average, i.e., they cannot be employed to transport a continuous phase. One exception is the motion of magnetic particles in ferrofluids under the influence of an oscillating magnetic field [4]. There the resulting net motion of the particles is transmitted to the carrier liquid by a strong viscous coupling.

However, the basic concept of ratchet transport – that a locally asymmetric but globally homogeneous system may induce global transport if it is kept out of equilibrium [5] – applies equally well to pure continuous media. This has been employed recently to transport a liquid or a solid phase in settings that do not show any macroscopic gradient [6–8]. The local asymmetry can result, for instance, from a periodic but asymmetric external potential. The periodic asymmetric variation needs to be on a small length scale compared to the system size.

In a first example, drops that are either placed on an asymmetrically structured substrate or between two such substrates move on average if a transverse electric field is applied periodically [8]. A similar transport may be achieved by vibrating the structured substrate in a tangential direction [8]. A second example is the triggering of a large scale mean flow in Marangoni–Bénard convection over a solid substrate with asymmetric grooves [6]. That is an interesting example (that has not yet been studied in detail theoretically) as the static ratchet profile of the substrate interacts with the time-periodic motion of the convection rolls to produce the mean flow, i.e., the time-periodic 'switching' is done by the system itself. The strength and direction of the mean flow depend on the thickness of the liquid layer and the applied temperature gradient across the layer. A third example are Leidenfrost drops that are placed on a hot surface with a ratchet-like topography. This induces a directed motion of the drops [7,9]. The effect is not only observed for many liquids but as well for small blocks of dry ice [10].

In contrast to the case of particle ratchets, not many models exist for the ratchet-driven transport of a continuous phase. Ref. [11] considers a channel flow that is induced by locally asymmetric periodic arrays of electrodes under an AC voltage [12], and proposes an electro-osmotic model.

A different concept was analysed in relation to the first experimental example: a two-layer film confined between two parallel plates can be driven by periodically switching on and off an external potential that is of ratchet shape in space. In the case that the potential is an electrical one and the two plates form a (heterogeneous) capacitor one may call the setup a flashing '(electro-) wettability ratchet' [13,14]. The concept of wettability may be

* Corresponding author. Tel./fax: +44 (0) 1509 223 186/969.
E-mail address: u.thiele@lboro.ac.uk (U. Thiele).
URL: http://www.uwethiele.de (U. Thiele).

0301-0104/$ - see front matter © 2010 Elsevier B.V. All rights reserved.
doi:10.1016/j.chemphys.2010.07.011

understood in a rather general way as it may include any effective interactions between the liquid–liquid free interface and the solid walls as long as one is able to apply them in a time-periodic, spatially periodic (but locally asymmetric) manner.

Net transport of a continuous phase may not only be caused by an external ratchet potential, but also by a self-ratcheting effect: An enlightening example are drops that are driven up an incline by harmonic substrate vibrations at a finite angle to the substrate normal [15,16]. A simple ratchet-like mechanism has been proposed [17]: The vibration component that is orthogonal to the substrate strongly modulates the hydrostatic pressure and thereby induces a nonlinear response in the drop shape. That in turn determines the strongly nonlinear drop mobility. As a result the drop reacts in an asymmetric manner to the vibration component parallel to the substrate. This symmetry breaking between back and forth motion leads to the observed net motion of the drop. A second experiment does not employ an oblique vibration but decouples the normal and parallel vibrations entirely [18]. On a horizontal substrate a net transport may be induced in either direction depending on the phase shift and amplitude ratio of the two harmonic vibrations. Note, that in Ref. [18] both vibrations have the same frequency. In both vibration experiments the phenomenon might be seen as a rocked self-ratcheting [1] of the drop as it is the drop itself that introduces the local time-reflection asymmetry in the response to the time-periodic driving of the sliding motion.

The decisive element in both presented systems – the ratchet capacitor and the vibrated drop – is the interaction of the external periodic forces with capillarity and wettability. With other words the nonlinearity that is necessary for a net motion results from interface effects. We propose to call this class of ratchets, 'interfacial flow driven ratchets'. As the resulting mean flow results from nonlinear interface effects they may become more effective the smaller the involved scales are. This implies that they are good candidates for micro- or even nano-fluidic actuators.

In the present contribution we will restrict our attention to one-layer films (i.e., liquid under gas) and formulate the thin film model that applies to both driving types – an external ratchet potential and the vibration (Section 2). Then we present selected results for the external electrical ratchet potential in Section 3. Section 4 discusses drop transport by an oblique vibration of the substrate (cf. [15]), whereas Section 5 describes results for the recently investigated case where the drop moves as a reaction to a phase shift between decoupled horizontal and vertical vibrations [18]. Finally, we conclude and give an outlook in Section 6.

2. Long-wave film profile evolution equation

We restrict our attention to a two-dimensional system and consider films/drops on lengthscales in the micrometer range. The behaviour is then controlled by the interplay of the time-periodic external force (and its spatial modulation), wettability and capillarity. In the limit of small surface slopes (small contact angles) it can be well described using an evolution equation for the film thickness profile $h(x,t)$ that is derived from the momentum transport equations with adequate boundary conditions employing long-wave approximation [19,20]. In dimensionless form we find

$$\partial_t h = -\partial_x\{Q(h)\partial_x[\partial_{xx}h + P(h,x,t)] + Q(h)F(t)\}. \quad (1)$$

As mass is conserved (no evaporation is considered), the time derivative of the film thickness profile equals the divergence of a flow. The flow results from a pressure gradient and a lateral force and is proportional to a mobility $Q(h)$. The pressure contains the Laplace or curvature pressure and a term $P(h,x,t)$ that stands for all other pressure contributions as, e.g., disjoining pressure (wettability), hydrostatic pressure, electrostatic pressure and so on. The pressure P might depend on position and time. The lateral driving force F may include gravity (drop on incline), thermal or wettability gradients and other. Depending on the particular effect included it might as well depend on h.

We are here particularly interested in three cases:

(i) For a liquid film in an external electrical ratchet potential on a horizontal substrate one has

$$P(h,x,t) = \Pi_{vdW}(h) + \Omega(t)\Phi(x)\Pi_{el}(h) \quad (2)$$

and $F = 0$. The disjoining pressure Π_{vdW} comprises the effective interactions between the liquid–gas interface and the substrate, i.e., the wettability properties [21,22,19]. We assume that a dielectric oil forms a film in a capacitor of gap width d. The oil wets the lower plate and does not wet the upper plate corresponding to

$$\Pi_{vdW} = \left(\frac{A_l}{h^3} + \frac{A_u}{(1-h)^3}\right) \quad (3)$$

with the dimensionless Hamaker constants $A_l > 0$ and $A_u < 0$. The dielectric film is subject to an electrical 'disjoining' pressure [23,24]

$$\Pi_{el} = \frac{(\varepsilon_r - 1)}{[\varepsilon_r + (1-\varepsilon_r)h]^2} \quad (4)$$

that varies in space as described by $\Phi(x)$ and is periodically switched in time as $\Omega(t)$. In Eq. (4), ε_r denotes the ratio of the relative dielectric constants of the liquid, ε_{liq}, and the gas phase, ε_{air}. The function $\Phi(x)$ models an electric field that is periodic in x, but with an asymmetric profile, i.e., there exists no reflection-symmetry in x. The employed spatial variation $\Phi(x)$ and the temporal modulation $\Omega(t)$ are defined by the sketches in Fig. 2(d) and (e), respectively.

The introduced scales are $3\gamma\eta/d\kappa_{el}^2$, $\sqrt{\gamma d/\kappa_{el}}$, and d for time t, position x, and film thickness h, respectively. Thereby, we have defined an electrostatic 'spreading coefficient' $\kappa_{el} = \varepsilon_0\varepsilon_{\text{liq}}U^2/2d^2$ where ε_0 is the absolute dielectric constant and U is the applied voltage. γ and η denote surface tension and dynamic viscosity of the liquid, respectively.

For simplicity we assume $A_l = -A_u = A > 0$. The dimensionless Hamaker constant A is related to the dimensional one by $A = A_{\text{dim}}/6\pi d^3\kappa_{el}$. To characterise the ratchet we introduce the flashing ratio $\chi = \tau/(T-\tau)$ and the asymmetry ratio

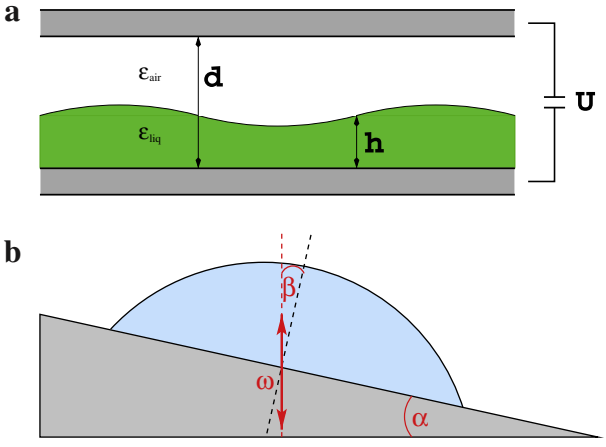

Fig. 1. (a) Sketch of a film of dielectric liquid of thickness $h(x)$ in a capacitor of gap width d and voltage $U(x,t)$. The relative dielectric constants of the liquid and air are ε_{liq} and ε_{air}, respectively. (b) Sketch of a drop on a vibrating inclined substrate. The frequency and angle of the vibration with the substrate normal are ω and β, respectively. The inclination angle of the substrate is α.

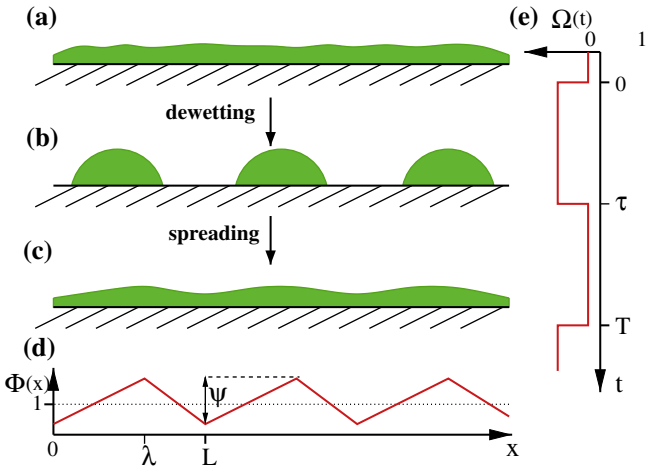

Fig. 2. Panels (a)–(c) illustrate the working principle of a fluidic ratchet based on a switchable wettability that causes dewetting-spreading cycles. (d) illustrates the spatially asymmetric periodic interaction profile $\Phi(x)$ responsible for the wettability pattern and (e) indicates the time-dependence $\Omega(t)$ of the switching in relation to the dewetting and spreading phases in (a)–(c).

$\phi = \lambda/(L-\lambda)$. The flashing frequency is $\omega = 2\pi/T$. The net transport along the substrate is measured by the mean flow $\langle j \rangle$. For more details see [13,14].

(ii) In the second example we look at drop transport by an oblique vibration that determines both, P and F [17]. The pressure

$$P(h,x,t) = \Pi(h) - Gh[1 + a(t)] \tag{5}$$

contains the disjoining pressure $\Pi(h) = -1/h^3 + 1/h^6$ and the hydrostatic pressure where the time-dependence results from the vibration component normal to the substrate. Π contains long-range destabilising and short-range stabilising van der Waals interactions [25]. The lateral force

$$F = G[\alpha + \beta b(t)] \tag{6}$$

contains a constant part (force down the incline) and a time-modulated part (vibration component parallel to the substrate). For a harmonic oblique vibration, the substrate acceleration is $a(t) = b(t) = a_0 \sin(\omega t)$. Note, that the physical vibration angle is $O(\theta_e \beta)$ where θ_e is the mesoscopic equilibrium contact angle, i.e., a scaled angle β of order one corresponds to a small physical angle.

In this case, the introduced scales are $3\gamma\eta/h_0\kappa^2$, $\sqrt{\gamma h_0/\kappa}$, and $h_0 = (B/|A|)^{1/3}$ for time t, position x, and thickness h, respectively. $A < 0$ and $B > 0$ are the Hamaker constants for the long- and the short-range part of the disjoining pressure, respectively. Furthermore, $\kappa = |A|/6\pi h_0^3$, and $G = \rho g h_0/\kappa$, where ρ denotes the density of the liquid and g the gravitational acceleration. The non-dimensional vibration period is $T = 2\pi/\omega$. The fixed drop volume $V = L(\bar{h} - h_p)$ is determined by the domain size L, the mean film thickness $\bar{h}$ and the dimensionless precursor film thickness $h_p = 1$. The resulting transport along the substrate is measured after all transients have decayed and the vibration-induced shape changes of the drop are completely periodic in time. We quantify the transport by the mean drop velocity $\langle v \rangle = \Delta x/T$ where Δx denotes the distance the drop moves within one period T.

(iii) The final example is closely related to the second one. In the experiments of Ref. [18] the normal and lateral substrate vibrations are mechanically decoupled and may have different amplitudes, frequencies and phases, i.e., the normal vibration in Eq. (5) is $a(t) = a_0 \sin(\omega_a t + \delta)$, and the lateral one in Eq. (6) is $\beta b(t) = \beta a_0 \sin(\omega_b t)$. In the particular case of [18], a horizontal substrate is used, i.e., $\alpha = 0$ and $\omega_b = \omega_a = \omega$. The parameter β takes the role of the ratio of the vibration amplitudes in the directions parallel and normal to the substrate. To be consistent with the long-wave approach taken, the physical amplitude ratio has to be small. However, as in (ii) β is the scaled ratio and therefore of $O(1)$.

3. Flow in a ratchet capacitor

Fig. 2 sketches an idealised electrical wettability ratchet. The working principle is as follows. The flat free surface of a film of a dielectric liquid that wets the lower wall of the capacitor is stable when the electric field is switched off (Fig. 2(a)). When switching on the spatially inhomogeneous electric field at $t = 0$ (see spatial profile and time-dependence in Fig. 2(d) and (e), respectively) the film dewets the substrate and decays into a set of drops (we call this the 'on-phase'). This is due to a destabilisation of the surface by the overall electric field *and* its gradients parallel to the substrate (Fig. 2(d)). The latter interfere with the wavelength selection in the linear phase of the surface instability. They do as well accelerate the coarsening process. The different processes during the on-phase can be well appreciated in Fig. 3. The qualitative behaviour in the on-phase of the cycle resembles dewetting of a liquid film on a substrate with a chemical wettability pattern [26,27]. If the on-phase is long enough (as is the case in Fig. 3) all the liquid collects in drops close to the positions of the maximal voltage (Fig. 2(b)). Then the field is switched off ('off-phase') at $t = \tau$ (Fig. 2(e)) and the drops spread (Fig. 2(c)), merge and become a homogeneous film again (Fig. 2(a)). The next cycle starts at $t = T$. If the period of the cycle is not large enough, the surface may not become entirely flat, a small modulation remains as indicated in Fig. 2(c).

When initially switching on the device there are several cycles (typically ~5–50, the number varies with the employed parameters) that show transient behaviour. However, the initial transients die out and the evolution of the film profile during one cycle is exactly time-periodic. Note, that there exist small parameter ranges where this is not the case due to resonance phenomena and/or multistability of various film states. However, this shall not concern us here.

Although the evolution of the film profile is exactly time-periodic, the process re-distributes the liquid within the film. This results in a net transport that depends in a non-trivial way on the various control parameters. As an example we give in Fig. 4 a log–log plot of the dependence of the mean flux on the flashing frequency. For the used flashing ratio and ratchet geometry the flux is always positive and approaches zero in the zero frequency limit as well as in the high frequency limit. For large frequencies the fluid does not have enough time to dewet in the on-phase or to spread in the off-phase. At small frequencies both processes reach the respective equilibrium well before the next switching, i.e., most time is spend waiting. As a result the mean flow increases proportionally with frequency when increasing the frequency from zero (cf. Fig. 4). The flux reaches a maximum at $\omega = 10^{-3}$–10^{-2} before it decreases again. The decrease seems to follow a power law as well. It is, however, not universal: the exponent increases with increasing mean film thickness. The decaying part shows non-monotonic step-like behaviour that is more pronounced for smaller film thicknesses. This results from that fact that films of smaller thicknesses dewet in a homogeneous electric field with a wavelength well below the spatial period of the ratchet. The more wavelengths fit into a ratchet period the more coarsening steps can take place in the on-phase if the frequency is small enough. Each of the 'steps' in the curves of Fig. 4 is related to a coarsening step that does not take place above the frequency at the step. At smaller mean film thicknesses the maximum resembles a plateau with a flux that does nearly not change between $\omega = 10^{-3}$ and 10^{-2}. The maximal flux increases with increasing mean film thickness. The

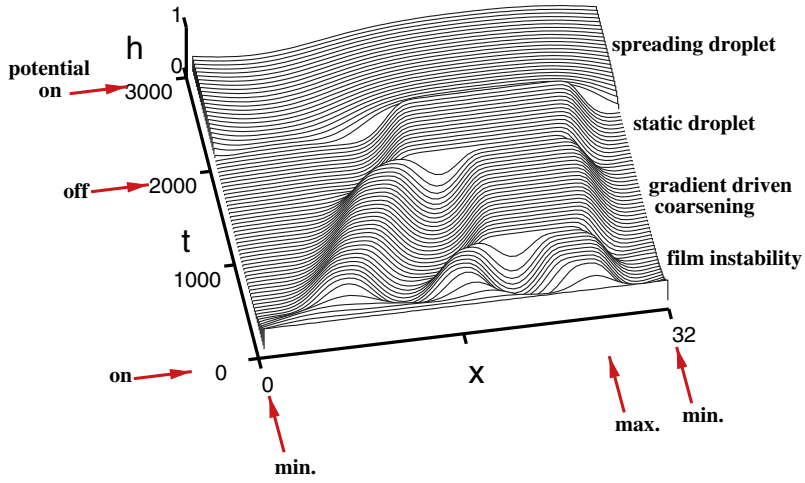

Fig. 3. Shown is a space–time plot of the typical evolution of the film thickness profile of a film of dielectric liquid in a heterogeneous capacitor (one spatial period shown) during one flashing period. For capacitor geometry and flashing cycle see Fig. 2. Parameters are $\bar{h} = 0.5$, $\Psi = 0.5$, $L = 32$, $\phi = 5$, $T = 5000$, $\chi = 1$, $A = 0.001$, $\varepsilon_r = 2.5$. The starting time is well after initial transients have decayed.

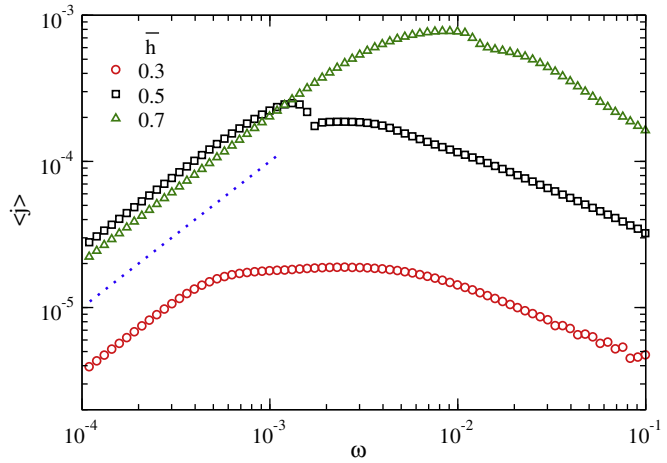

Fig. 4. Shown is the net transport as measured by the mean flux $\langle j \rangle$ in its dependence on the flashing frequency ω for various film thicknesses as indicated in the legend. The remaining parameters are as in Fig. 3. The dotted straight line corresponds to a power law of exponent one.

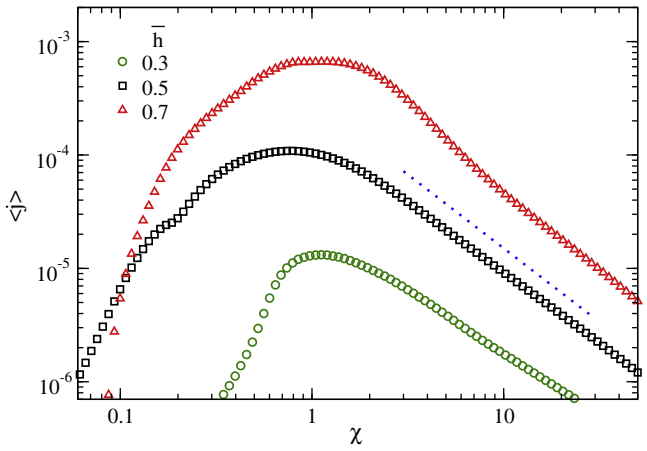

Fig. 5. Shown is the net transport as measured by the mean flux $\langle j \rangle$ in its dependence on the flashing ratio χ for various film thicknesses as indicated in the legend. $T = 500$ and the remaining parameters are as in Fig. 3. The dotted straight line corresponds to a power law of exponent −1.3.

particularly interesting non-monotonic behaviour close to the flow maximum (here well visible for $\bar{h} = 0.5$) results from the interaction of the dynamics of the 'last' coarsening step and the switching cycle.

Second, Fig. 5 shows the dependence of the mean flux on the flashing ratio. When it is low, i.e., the ratchet is most of the time in the off-phase, the flux is very low. This is because the liquid remains nearly homogeneously spread out as it has no time to assemble at the points of maximal voltage. By increasing the time of the on-phase the flux increases in a non-trivial manner until it reaches a maximum at $\chi \approx 1$. Depending on the film thickness one may find almost a plateau, i.e., a range of flashing ratios with nearly constant flux. For high flashing ratios the flux decreases again, since the ratchet is most of the time in the on-phase. That implies electrically formed drops have not enough time to spread out. The decrease follows a power law with an exponent of about −4/3.

Further calculations (not shown) indicate that the mean flux increases monotonically with increasing spatial asymmetry ratio ϕ and the amplitude Ψ of the ratchet potential. Note that as expected the net transport is zero at $\phi = 1$, i.e., for a symmetric potential. For further results for the presented one-layer geometry, see Refs. [13,14]. Exchanging the air layer by a second dielectric liquid, one is able to transport the two liquids into opposite direction. There, depending on the ratios of the viscosities and relative dielectric constants one may as well find a flux reversal. This is further discussed in Ref. [14]. With this we close our present discussion of case (i), i.e., the study of the transport of a dielectric liquid by a ratchet capacitor. Our results are typical for many externally imposed ratchets. The two cases discussed next are both related to net transport through substrate vibrations. Note that they can be seen as 'intrinsic' or self-inflicted ratchets.

4. Drop transport by oblique substrate vibration

As the first case of vibration-induced transport we discuss case (ii) introduced in Section 2 – a drop transported by an oblique substrate vibration as sketched in Fig. 1(b) and experimentally observed in Ref. [15]. The present results extend the ones of Ref. [17]. The typical behaviour of a drop during one vibration cycle

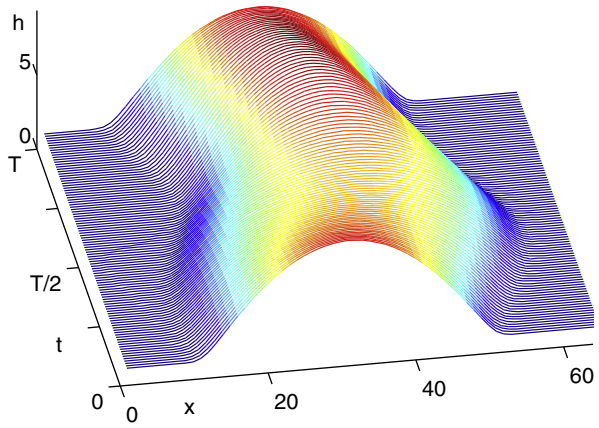

Fig. 6. Space–time plot illustrating the evolution of the profile of a drop on a obliquely vibrated substrate during one vibration period. Each cycle results in the net motion of the drop to the left. The starting time is well after initial transients have decayed. Note that only part of the domain L is shown. Parameters are $V = 192$, $G = 0.001$, $\beta = 0.1$, $\alpha = 0$, $T = 400$ ($\omega \approx 0.017$), $L = 128$, $a_0 = 10$.

as obtained in a time simulation of Eq. (1) is given in Fig. 6. One observes that the drop undergoes changes of shape and moves back and forth. Such simulations in time may be employed to analyse the net transport over a wide frequency range. In addition one may use continuation techniques [28–30] to study the behaviour in the low frequency limit, i.e., for a slowly vibrating substrate. In this limit the intrinsic timescale of the drop dynamics t_0 is much smaller than the vibration period T and the drop moves in a quasi-stationary manner. This means that drop shape and velocity at each instant during the vibration cycle correspond to the ones of a stationary moving drop at the corresponding constant force. They are parametrized by $a(t)$. Averaging stationary drop velocities $v(a(t))$ over one vibration period gives the low frequency limit of $\langle v \rangle$.

Fig. 7 presents results for the low frequency limit. Panel (a) shows profiles of stationary moving drops at various phases of the cycle on a horizontal substrate. Panels (b) and (c) give drop velocity and the dynamic mesoscopic contact angles, respectively, over one vibration cycle. The angles are shown for the left (θ_l) and right (θ_r) contact line. In the given setup, temporal modulations of the right contact angle are larger than those of the left one. The deviation of the velocity of the sliding drop from a harmonic modulation (dotted line in Fig. 7(b)) is a measure of the net motion of the drop.

The overall behaviour of the drop over one vibration cycle is very similar in Fig. 6 (finite, but small frequency) and Fig. 7 (low frequency limit): during the first half of the cycle ($t < T/2$) the drop is flattened and moves to the right. Note that this happens when the substrate is accelerated upwards and to the left. In the second half of the cycle the drop becomes taller and less wide while it slides to the left ($t > T/2$, substrate acceleration is downward and to the right). After one period the drop has moved a small net distance to the left. For the parameters of Fig. 6 it takes about 100 vibration cycles to move the drop by its own length. As detailed below in the conclusion, this does well correspond to the available experimental results [15].

Based on the described findings one is able to understand the mechanism that leads to the net motion of the drop: The component of the oblique vibration that is normal to the substrate strongly modulates the hydrostatic pressure and therefore provokes a nonlinear response in the drop shape, i.e., when the substrate accelerates upwards [downwards] it compresses [decompresses] the drop. That in turn determines the strongly nonlinear drop mobility $Q(h)$ in Eq. (1) and is therefore responsible for an asymmetric response to the back and forth forcing that results from the parallel vibration component. As a result of this nonlinear coupling of the effects of normal and parallel vibration component one obtains an anharmonic response of the drop to the harmonic but oblique vibration.

The examples given in Figs. 6 and 7 where for a rather small vibration angle β. Therefore the change in drop shape was mainly due to the modulation of the hydrostatic pressure. For larger β the drop additionally changes its shape in response to the parallel vibration component. An examples is given in Fig. 8. The characteristic backwards shoulders are known from strongly driven drops on homogeneous substrate [31,30]. For even larger β the process

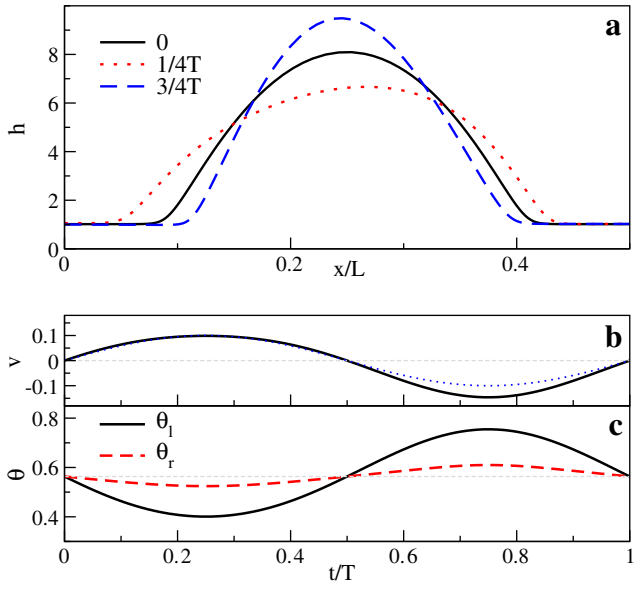

Fig. 7. Shown are for an obliquely vibrated horizontal substrate in the low frequency limit, (a) several drop shapes at times as given in the legends, (b) the momentaneous velocity, and (c) the left (θ_l) and right (θ_r) mesoscopic dynamic contact angle during one vibration cycle. For the used $\beta = 0.3$ the drop moves with $\langle v \rangle \approx -0.01$, i.e., to the left. The blue dotted line in (b) indicates a harmonic variation of zero net flow. Remaining parameters are as in Fig. 6. (For interpretation of the references in colour in this figure legend, the reader is referred to the web version of this article.)

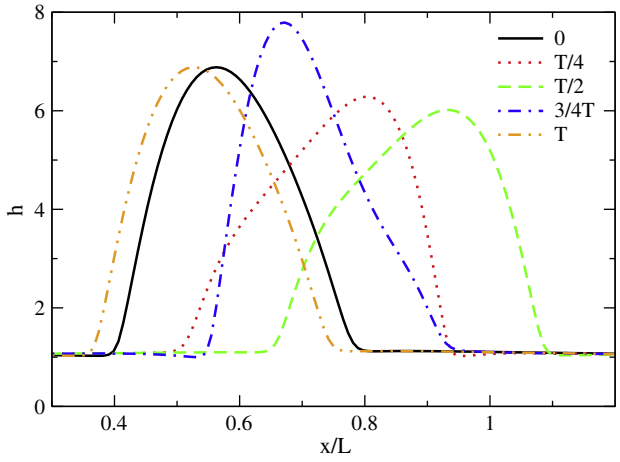

Fig. 8. Shown are several drop shapes during one vibration cycle for an obliquely vibrated horizontal substrate at $V = 192$, $G = 0.001$, $a_0 = 10$, $\alpha = 0$, $T = 400$, $L = 128$ and a relatively large vibration angle $\beta = 1$.

may become very complicated as the drop can during a single cycle undergo several morphological changes. It can transform between a spherical cap-like drop via a drop with a backwards shoulder to a finite film with a capillary rim [31]. We do here, however, not investigate this regime further.

For smaller vibration angles β morphological transitions do not occur (at reasonable accelerations a_0). This allows for 'universal' behaviour, i.e., one finds that scaling laws that are discovered in the low frequency regime hold in part in the entire frequency range studied. In particular, one finds in the low frequency regime a scaling $\langle v\rangle \sim \beta a_0^2 L^{1.67}$. Fig. 9(a) shows that for drops of identical volume the scaling $\langle v\rangle \sim \beta a_0^2$ does hold very well as it is possible to 'collaps' curves for a range of parameter pairs (a_0, β) on a single master curve. The scaling with volume does, however, not hold (see Fig. 9(b)). Interestingly, one finds a flux reversal at high frequencies, i.e., above a critical frequency ω_c the drops move on average to the right. Fig. 9(b) further indicates that for larger drop volume the reversal is more pronounced and occurs at lower frequencies ω_c. We will end this section with an investigation of the origin of the reversal.

To this end we show in Fig. 10 a superposition of drop profiles obtained at frequencies above and below ω_c at selected times during the vibration cycle. The profiles in the low frequency limit are per definition ideally in-phase with the substrate vibration. At $T = 400$ ($\omega = 0.016 < \omega_c \approx 0.05$, cf. Fig. 9(b)) the profiles near the times of maximal acceleration (i.e., $t \approx T/4$ and $t \approx 3T/4$) strongly resemble the ones in the low frequency limit, although the variation in their shape is already smaller. For $T = 1000$ they are nearly indistinguishable (not shown). However, around $t = 0$ and $T = T/2$ where the acceleration changes sign the convergence to the low frequency limit is much slower as there even small phase lags are very important (cf. Fig. 11). The overall behaviour can be well appreciated in Fig. 11 where the dependence of the maximal drop height on time is shown for one vibration cycle for several different periods. With decreasing period we observe a continuous increase of the phase shift w.r.t. the curve for the low frequency limit. The curves of finite frequencies lag behind the one for zero frequency and show a less pronounced variation of the drop heights.

At $T = 70$ ($\omega = 0.090 > \omega_c$) the drop profiles in Fig. 10 vary much less over time than for the lower frequencies and Fig. 11 shows a rather large phase shift (larger than $\pi/3$) as compared to the other curves. When increasing the frequency, due to the phase shift and nonlinear mobility eventually the average response to the backwards force becomes smaller than the one to the forward force and the drop shows a reversal of the net motion. The net motion to the right becomes maximal at an optimal frequency. The influence of the phase lag still exists at higher frequencies, however, as the changes in the profile shape become smaller with increasing frequency, the mean velocity decreases again and approaches zero in the limit of large frequencies. This is as well the reason why the absolute values of the velocities that can be reached in the flow reversal regime are much smaller than the ones in the low frequency limit. Note, finally, that in the case of larger vibration angles the picture becomes more complicated as the phase lag interacts with the morphological changes. As a result the dependency of mean velocity on frequency might have more than one maximum.

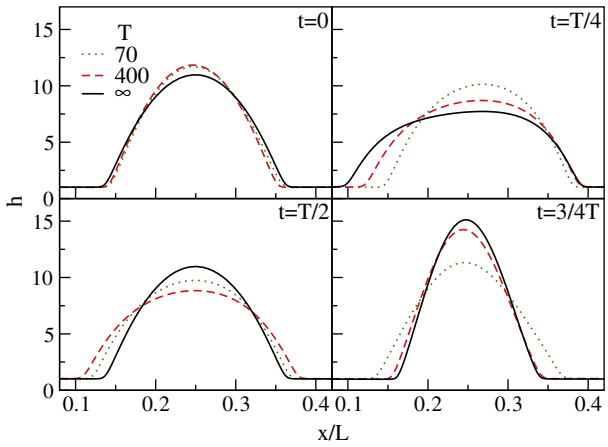

Fig. 10. Drop profiles at various times of the cycle as indicated in upper right corner of each plot for various vibration periods T as indicated in the legend. $T = \infty$ indicates the low frequency limit. Remaining parameters are $V = 384$, $L = 256$, $\alpha = 0$, $\beta = 0.1$, $a_0 = 10$, $G = 0.001$.

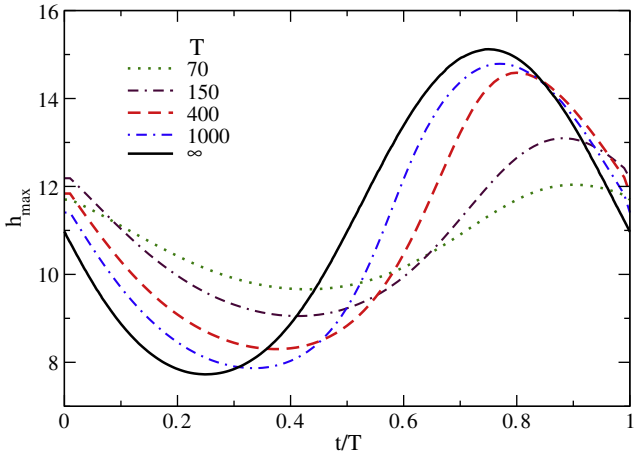

Fig. 11. Variation of the maximal drop height during one vibration period for different vibration periods as indicated in the legend. Remaining parameters are as in Fig. 10.

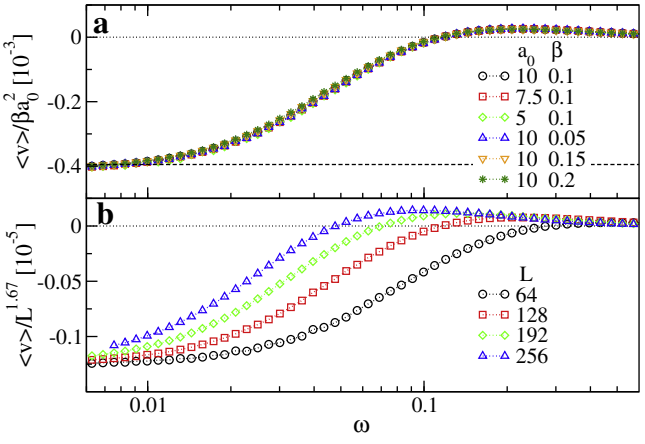

Fig. 9. Scaled mean velocity depending on the vibration frequency ω for drops on a horizontal substrate. Panel (a) gives the master curve for the scaled mean velocity $\langle v\rangle/\beta a_0^2$ for sets (a_0, β) as given in the legend. The horizontal dashed line indicates the result in the low frequency limit. Remaining parameters are as in Fig. 6. Panel (b) gives the scaled mean velocity $\langle v\rangle/V^{1.67}$ for drops of different volume as given in the legend. Remaining parameters are $a_0 = 10.0$, $\beta = 0.1$, $\alpha = 0.0$, $G = 0.001$.

5. Drop transport by decoupled horizontal and vertical substrate vibrations

As a second example of vibration-induced transport we discuss case (iii) introduced in Section 2 – a drop transported on a horizontal substrate by decoupled normal and parallel substrate vibrations

as experimentally observed in Ref. [18]. We focus on normal and parallel vibrations of identical frequency that have a phase shift and possibly different amplitudes. Following the discussion of the underlying mechanism in case (ii) it is no surprise that a net motion is found with the present simple long-wave model as well for case (iii). Fig. 12 shows the dependence of the scaled mean velocity on the phase shift for different amplitude ratios β at a moderately large vibration period of $T = 200$ ($\omega = 0.031$). Very similar behaviour is found for other periods. Interestingly, the dependencies of the scaled velocity $\langle v\rangle/\beta$ for different β fall on a single master curve for $\beta \lesssim 0.2$. This implies that for $\beta \lesssim 0.2$ particularly important values of the phase shift do not depend on the amplitude ratio. In particular, we find that flow reversal occurs at $\delta = 3/4\pi$ and $\delta = 7/4\pi$. The drop moves fastest to the left [right] at $\delta = \pi/4$ [$\delta = 5/4\pi$]. The master curve shows the symmetry $(\delta \to \delta + \pi, \langle v\rangle/\beta \to -\langle v\rangle/\beta)$. Note that the symmetry holds for all considered amplitude ratios and periods (cf. Fig. 12), as can be expected from the setup of the problem.

However, the scaling found for small β does not hold for larger β (see Fig. 12). For $0.2 \lesssim \beta \lesssim 1.0$ the phase shift that results in maximal net motion and the maximal net velocity $\langle v\rangle$ both increase with increasing β. For $\beta \gtrsim 1.0$ both decrease again (not shown). This implies that the amplitude ratio that maximises net transport is $\beta = 1$. There the phase shift resulting in maximal net transport to the left is slightly smaller than $\delta = \pi/2$.

The change of the dependency of transport on phase shift with changing period is shown in Fig. 13. In accordance with results in case (ii) one finds that the velocities become monotonically smaller (for all phase shifts) with increasing frequencies (decreasing periods) as the drops are less able to follow the substrate vibrations. The phase shift where the maximal mean velocity occurs becomes smaller with decreasing frequencies. In the limit of low frequency the fastest transport to the left and right are found at $\delta = 0$ and $\delta = \pi$, respectively.

A comparison with the experiments in Ref. [18] (in particular their Fig. 3) shows that there the phase shift value where the maximal mean velocity is found and the value of the maximal mean velocity both increase with increasing ratio of the amplitudes of parallel and normal vibration. However, as further explained in the conclusion, a direct quantitative comparison is not possible. The experimental results show roughly the symmetry $(\delta \to \delta + \pi, \langle v\rangle \to -\langle v\rangle)$. Small deviations are explained by the presence of defects on the substrate [18] (see, in particular, the inset of their Fig. 2). A striking difference between the results presented here and Fig. 3(a) of [18] is that in the latter the mean velocity depends in a strongly non-harmonic way on the phase shift. In the simulations we have not seen the experimentally found double peak structure around the maximal velocity. This point needs further investigation.

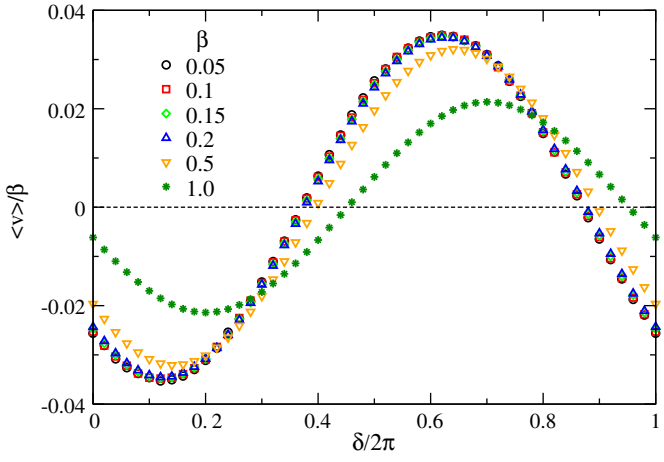

Fig. 12. Shown is the mean velocity as a function of the phase shift δ for various amplitude ratios β as given in the legend. Thereby, we use a relatively large period of $T = 200$ and give the scaled velocity $\langle v\rangle/\beta$. For $\beta \lesssim 0.2$ all curves 'collapse' onto a master curve. The remaining parameters are $V = 192$, $G = 0.001$, $a_0 = 10$, $\alpha = 0$, $L = 128$, $a_0 = 10$.

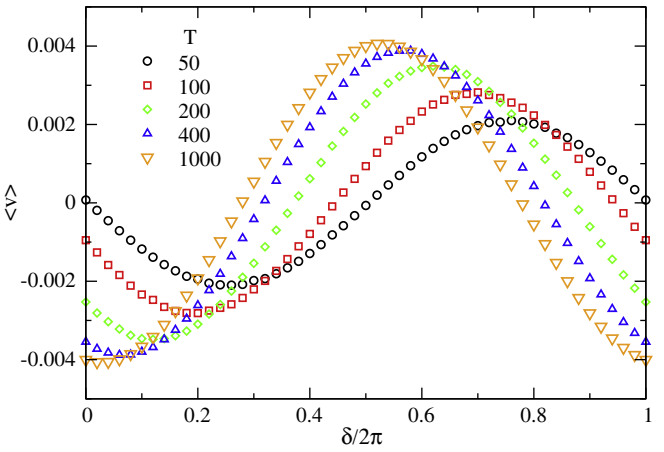

Fig. 13. Shown is the mean velocity as a function of the phase shift δ for various periods as given in the legend. The remaining parameters are $V = 192$, $G = 0.001$, $a_0 = 10$, $\beta = 0.1$, $\alpha = 0$, $L = 128$, $a_0 = 10$.

6. Conclusions

We have explored the usage of ratchet mechanisms to transport a continuous phase in micro-fluidic settings involving a free liquid–gas interface and contact lines, i.e., under the influence of capillarity and wettability. In particular, we have studied on the one hand the transport of a dielectric liquid in a capacitor with an asymmetrically spatially modulated electrical field that is periodically switched on and off. In this case the ratchet-like potential is imposed externally. On the other hand we have investigated drops on a solid substrate that show net motion under the influence of different types of harmonic substrate vibrations. Analysing the underlying mechanism we have found that the component of the harmonic vibration that is orthogonal to the substrate induces a nonlinear (anharmonic) response in the drop shape. The latter determines the strongly nonlinear drop mobility what results in an asymmetric response of the drop to the vibration component that is parallel to the substrate. The induced symmetry breaking between forward and backward motion during the different phases of the vibration results in the observed net motion of the drop. We have argued that the phenomenon might be seen as a rocked self-ratcheting as the drop itself introduces the local time-reflection asymmetry in the response to the time-periodic driving of the sliding motion. We employ the term 'rocked' as the net motion is strongest in the low frequency limit as is typical for rocked particle ratchets [1]. Note as well that in the context of a drop on an incline the component of the vibration parallel to the substrate can be seen as a periodic rocking of the substrate.

For the vibrated drops our focus has been on two experimentally realised cases [15,16,18]: an oblique substrate vibration and decoupled normal and parallel substrate vibrations of identical frequency but different amplitudes and/or phase shifts. As in the latter case the use of different amplitudes without phase shift corresponds to the case of the oblique vibration we have mainly analysed the dependence of the drop motion on phase shift.

In both presented systems – the ratchet capacitor and the vibrated drop – the net motion results from nonlinearities related to interface effects, in particular (electro-) capillarity and wettability. Therefore we propose to name this class of ratchets 'interfacial flow driven ratchets'. As interface effects dominate, these ratchets become more effective the smaller the involved scales are, because in the case of capillarity the ratio of surface to volume forces scales as $L^2/L^3 = 1/L$ where L is a typical length scale of the system. This implies that the interfacial flow driven ratchets may be good candidates for micro- or even nano-fluidic actuators.

One has, however, to add a word of caution. Efficiency of the interfacial flow driven ratchets does not follow a simple universal scaling law as various other effects enter in the different stages of the ratchet cycles. In all cases wettability plays a role. In case (i) we consider a stabilizing ($\sim h^{-3}$) van der Waals force that determines the spreading stage. In cases (ii) and (iii) destabilizing ($\sim h^{-3}$) and stabilizing ($\sim h^{-6}$) van der Waals forces introduce a small length scale h_0, which corresponds to a precursor or wetting layer film thickness that is (nearly) not affected by the typical droplet size and dynamics. This length enters the ratio of the forces due to the substrate vibration and the surface forces (cf. Section 2). The vibrated droplet ratchet works better if the ratio is not very small.

One also needs to keep in mind that all models analysed in the present contribution are obtained employing a long-wave or lubrication approximation [19,20]. That means they are relatively simple – but fully dynamical – highly nonlinear models based on a minimal set of ingredients, i.e., Stokes flow in the lubrication approximation, (electro-) capillarity, and wettability. They allow to study the net transport in the ratchet capacitor and the net motion of the vibrated droplet over a wide range of parameters, to understand the underlying mechanisms and to discuss transitions in the qualitative system behaviour.

However, when comparing such lubrication models with particular experiments one always has to keep in mind that the formal range of applicability of the lubrication approximation is limited and does often not overlap with the parameter ranges where experiments work best. The latter are often performed with liquid-substrate combinations that lead to equilibrium (and dynamic) contact angles that are not small. In our case (ii) one uses as well large substrate inclinations and large angles between vibration direction and substrate normal. For a direct quantitative comparison *all* those angles have to be small. Nevertheless, lubrication models are extremely successful in explaining intriguing effects observed in a wide range of experiments involving capillarity and wettability. A good example for this are studies of morphological changes in sliding drops where some experiments are done for liquids with static contact angles above $\pi/4$ using substrate inclinations varying from zero to $\pi/2$ [32]. Lubrication theory well explains the effects (see, e.g., [33] and the discussion in [34]).

For the vibrated drop in Ref. [15] a liquid is used that has an equilibrium contact angle of about $\pi/3$, the substrate inclination is $\pi/4$, and the vibration is applied at an angle of $\pi/4$ with the substrate normal, i.e., the experiment is well outside the formal range of applicability of the lubrication approximation. Therefore, a direct quantitative comparison of mean velocities could only be done through some 'up-scaling' procedure that lifts drop volume, contact angles and vibration angle from the lubrication theory values to the experimental ones. This might be done (and is sometimes done). However, in our opinion the process has arbitrary elements, and we prefer not to employ it.

The theory may, however, be related to the experiment in a semi-quantitative way by comparing, for instance, mean velocity in terms of drop size or typical timescales. In Ref. [15] the employed frequencies f range from 25 Hz to 120 Hz. At an acceleration of 15 g and $f = 60$ Hz one finds mean velocities of about 1 mm/s, i.e., the drop moves less than 20 μm per cycle. For a drop of 3 mm length this implies that it needs about 150 cycles to move by its own length. The situation is very similar in Ref. [18] where for the parameters depicted in their Figs. 1 and 2 it takes about 50 vibration cycles to move the drop by its own length. Note, that their Fig. 1 does not show snapshots taken during a single cycle, but selected pictures from 70 cycles.

In terms of the number of cycles needed to move the drop by its own length our results are very close to the experimental findings: At a period of $T = 100$ we have a scaled velocity of about 0.1×10^{-3} (our Fig. 9(a)); for $a_0 = 10$ and $\beta = 0.2$ this gives $\langle v \rangle = 2 \times 10^{-3}$ and an advancement per cycle of $\Delta x = 0.2$. For a drop like the one in our Fig. 6 this implies that it takes about 190 cycles to move it by its own length. Employing instead the accelerations of 15 g as in [15] it takes about 90 cycles. This is a fair agreement between experiment and lubrication theory. One may as well discuss the time scale t_0 employed in the non-dimensionalisation and use it to compare the relevant vibration frequencies in the model and in the experiment.

Finally, we would like to discuss the relation of the discussed ratchet mechanisms to transport a continuous phase to 'particle ratchets'. We do this by pointing out some formal analogies between the employed thin film equation and a Fokker–Planck equation for transport of discrete objects in a particle ratchet.

The film thickness evolution equation

$$\partial_t h = -\partial_x \{ Q(h) \partial_x [\partial_{xx} h + P(h,x,t)] + Q(h) F(t) \}. \tag{7}$$

shows similarities to a Fokker–Planck equation for interacting particles in an external ratchet potential [35,36]. Its non-dimensional form is

$$\partial_t W = -\partial_x \{ W \partial_x P(W,x,t) + W F(t) \} \tag{8}$$

with

$$P(W,x,t) = -T(t) \log W - \tilde{g} W - U(x,t). \tag{9}$$

In the particular case, it is an evolution equation for the one-particle distribution function $W(x,t)$, where $U(x,t)$ is a flashing ratchet potential (note that the one used in [35,36] is static) 'rocked' periodically by $F(t)$. The function $T(t)$ stands for a periodic modulation of the non-dimensional temperature, and $\tilde{g}$ is a non-dimensional interaction parameter. One notes that both, the first order drift or transport term and the second order diffusion term are modulated in time. Note that $U(x,t)$ could as well be incorporated into the drift term instead of the diffusion term.

However, differing from [35,36] our cases (ii) and (iii) do not incorporate an external potential. The absence of a spatial ratchet potential is compensated by strongly nonlinear prefactors of the diffusion and the drift term that result in mean flow even for harmonic driving, i.e., for a driving that shows reflection-symmetry w.r.t. time. In the context of 'particle ratchets' related systems are studied where a mean flux is created without spatial ratchet potential but through the response of two different (weakly) coupled degrees of freedom to time-periodic driving [37,38]. The degrees of freedom are related to two different interacting particle species in [37], and to pancake vortices and Josephson vortices in layered superconductors in [38]. However, in contrast to our case in Refs. [37,38] the driving is time-asymmetric. Time-symmetric driving can as well induce mean transport in a 'particle ratchet' without spatially varying potential if the coupling of the different degrees of freedom is sufficiently nonlinear. Examples are the 'vortex diode' discussed in [39] and the rocked-pulsated ratchets that model a synchronized gating mechanism in [40,41]. Note finally, that similar 4th order terms as the capillarity term in Eq. (7) may be included in higher order Fokker–Planck equations.

Acknowledgment

This work was supported by the European Union under Grant PITN-GA-2008-214919 (MULTIFLOW).

References

[1] P. Hänggi, F. Marchesoni, Rev. Mod. Phys. 81 (2009) 387, doi:10.1103/RevModPhys.81.387.
[2] S. Matthias, F. Müller, Nature 424 (2003) 53.
[3] J. Rousselet, L. Salome, A. Ajdari, J. Prost, Nature 370 (1994) 446.
[4] A. Engel, H.W. Müller, P. Reimann, A. Jung, Phys. Rev. Lett. 91 (2003) 060602, doi:10.1103/PhysRevLett.91.060602.
[5] P. Curie, J. Phys. (Paris) 3 (1894) 393.
[6] A.D. Stroock, R.F. Ismagilov, H.A. Stone, G.M. Whitesides, Langmuir 19 (2003) 4358.
[7] D. Quéré, A. Ajdari, Nat. Mater. 5 (2006) 429.
[8] A. Buguin, L. Talini, P. Silberzan, Appl. Phys. A – Mater. Sci. Process. 75 (2002) 207.
[9] H. Linke, B.J. Alemán, L.D. Melling, M.J. Taormina, M.J. Francis, C.C. Dow-Hygelund, V. Narayanan, R.P. Taylor, A. Stout, Phys. Rev. Lett. 96 (2006) 154502, doi:10.1103/PhysRevLett.96.154502.
[10] G. Lagubeau, M. Le Merrer, C. Clanet, D. Quéré, Leidenfrost on a ratchet, Preprint.
[11] A. Ajdari, Phys. Rev. E 61 (2000) R45, doi:10.1103/PhysRevE.61.R45.
[12] A. Ramos, H. Morgan, N.G. Green, A. Gonzales, A. Castellanos, J. Appl. Phys. 97 (2005) 084906.
[13] K. John, U. Thiele, Appl. Phys. Lett. 90 (2007) 264102, doi:10.1063/1.2751582.
[14] K. John, P. Hänggi, U. Thiele, Soft Matter 4 (2008) 1183, doi:10.1039/b718850a.
[15] P. Brunet, J. Eggers, R.D. Deegan, Phys. Rev. Lett. 99 (2007) 144501, doi:10.1103/PhysRevLett.99.144501.
[16] P. Brunet, J. Eggers, R.D. Deegan, Eur. Phys. J. – Special Top. 166 (2009) 11, doi:10.1140/epjst/e2009-00870-6.
[17] K. John, U. Thiele, Phys. Rev. Lett. 104 (2010) 107801, doi:10.1103/PhysRevLett.104.107801.
[18] X. Noblin, R. Kofman, F. Celestini, Phys. Rev. Lett. 102 (2009) 194504, doi:10.1103/PhysRevLett.102.194504.
[19] A. Oron, S.H. Davis, S.G. Bankoff, Rev. Mod. Phys. 69 (1997) 931, doi:10.1103/RevModPhys.69.931.
[20] S. Kalliadasis, U. Thiele (Eds.), Thin Films of Soft Matter, Springer, Wien/New York, 2007, p. CISM 490.
[21] P.-G. de Gennes, Rev. Mod. Phys. 57 (1985) 827, doi:10.1103/RevModPhys.57.827.
[22] J.N. Israelachvili, Intermolecular and Surface Forces, Academic Press, London, 1992.
[23] Z. Lin, T. Kerle, S.M. Baker, D.A. Hoagland, E. Schäffer, U. Steiner, T.P. Russell, J. Chem. Phys. 114 (2001) 2377, doi:10.1063/1.1338125.
[24] D. Merkt, A. Pototsky, M. Bestehorn, U. Thiele, Phys. Fluids 17 (2005) 064104, doi:10.1063/1.1935487.
[25] L.M. Pismen, Phys. Rev. E 6402 (2001) 021603, doi:10.1103/PhysRevE.64.021603.
[26] K. Kargupta, A. Sharma, Phys. Rev. Lett. 86 (2001) 4536, doi:10.1103/PhysRevLett.86.4536.
[27] U. Thiele, L. Brusch, M. Bestehorn, M. Bär, Eur. Phys. J. E 11 (2003) 255, doi:10.1140/epje/i2003-10019-5.
[28] E. Doedel, H.B. Keller, J.P. Kernevez, Int. J. Bifurcat. Chaos 1 (1991) 493, doi:10.1142/S0218127491000397.
[29] E. Doedel, H.B. Keller, J.P. Kernevez, Int. J. Bifurcat. Chaos 1 (1991) 745, doi:10.1142/S0218127491000555.
[30] U. Thiele, K. Neuffer, M. Bestehorn, Y. Pomeau, M.G. Velarde, Colloid Surf. A 206 (2002) 87.
[31] U. Thiele, M.G. Velarde, K. Neuffer, M. Bestehorn, Y. Pomeau, Phys. Rev. E 64 (2001) 061601, doi:10.1103/PhysRevE.64.061601.
[32] T. Podgorski, J.-M. Flesselles, L. Limat, Phys. Rev. Lett. 87 (2001) 036102, doi:10.1103/PhysRevLett.87.036102.
[33] J.H. Snoeijer, N. Le Grand-Piteira, L. Limat, H.A. Stone, J. Eggers, Phys. Fluids 19 (2007) 042104, doi:10.1063/1.2722767.
[34] D. Bonn, J. Eggers, J. Indekeu, J. Meunier, E. Rolley, Rev. Mod. Phys. 81 (2009) 739, doi:10.1103/RevModPhys.81.739.
[35] S. Savel'ev, F. Marchesoni, F. Nori, Phys. Rev. E 70 (2004) 061107, doi:10.1103/PhysRevE.70.061107.
[36] S. Savel'ev, F. Marchesoni, F. Nori, Phys. Rev. E 71 (2005) 011107.
[37] S. Savel'ev, F. Marchesoni, F. Nori, Phys. Rev. Lett. 92 (2004) 160602, doi:10.1103/PhysRevLett.92.160602.
[38] D. Cole, S. Bending, S. Savel'ev, A. Grigorenko, T. Tamegai, F. Nori, Nat. Mater. 5 (2006) 305, doi:10.1038/nmat1608.
[39] S. Savel'ev, F. Nori, Nat. Mater. 1 (2002) 179, doi:10.1038/nmat746.
[40] S. Savel'ev, F. Marchesoni, P. Hänggi, F. Nori, Europhys. Lett. 67 (2004) 179.
[41] S. Savel'ev, F. Marchesoni, P. Hänggi, F. Nori, Phys. Rev. E 70 (2004) 066109, doi:10.1103/PhysRevE.70.066109.